TÜBİTAK

Turkish Journal of Earth Sciences
http://journals.tubitak.gov.tr/earth

Research Article

Turkish J Earth Sci
(2021) 30: 665-680
© TÜBİTAK
doi: 10.3906/yer-2102-11

Combined qualitative and quantitative regional interpretation of the thermal results of magnetic data in the Eastern Mediterranean Region

İlkin ÖZSÖZ
General Directorate of Mineral Research and Exploration, Ankara, Turkey

Received: 11.02.2021 **Accepted/Published Online:** 10.07.2021 **Final Version:** 28.09.2021

Abstract: The study presents thermal structure and active-passive tectonic parts of the Eastern Mediterranean Region. Curie point depth, heat flow map, Moho depth and sediment thickness are used for interpretation. The levelled magnetic data that obtained from the World Digital Magnetic Anomaly Map (WDMAM) is used. The magnetic anomaly is divided into 39 zones for Curie point depth estimation. The Curie point depth values are calculated into Fourier domain. Then heat flow map is generated. The estimated Curie point depth values are ranging from 4.5 km to 25 km. Furthermore, heat flow values are between 55 mW/m^2 and 277 mW/m^2. Moho depth, Moho depth-Curie depth and sediment thickness are used for constraining interpretation. Interpretation indicates that the northern and southern parts of the Mediterranean Ridge present different thermal characteristics.

Key words: Curie point depth, heat flow, thermal structure, East Mediterranean, Mediterranean Ridge

1. Introduction

It has been a long-lasting debate that how and when the deep East Mediterranean basins (Zohr, Herodotus, Ionian Basins, Levant and Sirte) formed. Even though the East Mediterranean Region is investigated by many researchers, the formation and tectonic evaluation is still arguable. The region is quite attractive for many researchers due to the hydrocarbon potential (Khain and Polyakova, 2004; Schenk et al., 2010; Eppelbaum et al., 2012; Hodgson, 2012). According to Schenk (2010), recoverable gas in the Levant Basin is roughly 4 trillion m^3. The combined geological and geophysical analysis provides more information about tectonic evaluation and hydrocarbon potential of the region.

Thermal structure of the Eastern Mediterranean can be analysed by estimated Curie depth from magnetic data. Typically, shallow Curie point depth (CPD) is associated with high heat flow and shallow crust depth. Nevertheless, Rozimant et al. (2009) indicated that the correlation between CPD, heat flow and crust depth may not be valid by reason of strongly magnetised rocks and isostasy. The thickness of the magnetic crust is associated with the CPD where remnant and induced magnetization of the magnetite disappears (Buddington and Lindsley, 1964; Gasparini et al., 1979; Nishitani and Kono, 1983; Hunt et al., 1995; Salazar et al., 2017). Curie temperature of magnetite is ranging from 575 °C to 590 °C (Hunt et al., 1995; Lowrie, 2007).

There were many studies conducted around the study area. Aydın et al. (2005) computed CPD of Turkey from aeromagnetic data. According to Aydın et al. (2005), estimated CPD is between 6 and 10 km in the Western Anatolia and roughly 25–30 km in the Southern part of the Anatolia. Pamukçu et al. (2014) estimated Curie point isotherm between 6 and 24 km and computed heat flow in the Eastern Anatolia. CPD in the central Anatolia is calculated by Ateş et al. (2005) and results are between 7.9 km and 22.6 km. Additionally, Hisarlı (1996), Dolmaz et al. (2005a), Dolmaz et al. (2005b), Salk et al. (2005), Bilim (2011), Maden (2012), Bilim et al. (2016), Bilim et al. (2017), Aydemir et al. (2018) and Aydemir et al. (2019) estimated and interpreted CPD within Turkey.

Recently, Elbarbary et al. (2018) proposed relation between CPD and seismic activity. Elbarbary et al. (2018) claimed that if CPD of the regions is shallower than 25 km, these areas are suitable for geothermal exploration and most of earthquakes are likely to originate in these zones. Shirani et al. (2020) computed CPD by de-fractal method in the northwest Iran. The results were fairly compatible with the resistivity profiles and well data. Erbek and Dolmaz (2019) mentioned the relationship between seismogenic zone and high heat flow areas which were derived from CPD calculations.

In this study, the thickness of the magnetic crust or CPD is calculated. Furthermore, estimated Moho depths are used for constraining interpretation. Generic Mapping Tools and Oasis montaj are used for mapping in this study. The aim of this paper is to reveal the regional thermal structure and magnetic crust thickness of the Eastern Mediterranean.

2. Tectonic setting

Eastern Mediterranean tectonism is formed by tectonic movements of African, Eurasian and Arabian plates. Compression in Eastern Anatolia and extension in Western Anatolia resulted in W-SW movement of the Anatolian Block (McKenzie, 1972; Le Pichon and Angelier, 1979; McClusky et al., 2000; Pamukçu, 2016; Kahveci et al., 2019). The major subduction along the Hellenic Subduction Zone stems from

* Correspondence: ilkin.ozsoz@mta.gov.tr

the roll-back system of the Aegean Sea, underlying the Mediterranean Slab (Le Pichon and Angelier, 1979; Le Pichon, 1983; Mercier e al., 1989).

Regarding the Western Anatolia, it can be said that the region is characterised by a considerably active extensional regime (McKenzie, 1978; Le Pichon and Angelier, 1979; Dewey et al., 1986; Jackson and McKenzie, 1988; Taymaz et al., 1990; Ambraseys and Jackson, 1990; Goldsworthy et al., 2002). There are various models (Dewey, 1988; Seyitoğlu and Scott, 1991; Dewey and Şengör, 1979; Le Pichon and Angelier, 1979) that explain the extensional regime in the Western Anatolia. The suggested models are: orogenic collapse, back-arc extension, tectonic escape model and combination of the three models.

The Eastern Mediterranean is characterised by complex tectonism which contains both terrain belts and oceanic rift systems (Stampfli et al., 2013). The region is part of the African-Eurasian collision zone (Ben-Avraham, 1978; Garfunkel, 1998). Simplified tectonic plates in the study area are illustrated in Figure 1. The major tectonic event that shaped the Eastern Mediterranean Sea is the Permian opening of the Neo-Tethys ocean (Schettino and Turco, 2011; Stampfli et al., 2001; Stampfli and Borel, 2002).

Tortonian (11.6 to 7.2 Ma), Messinian (7.2 to 5.3 Ma) and early Zanclean (5.3 to 5.0 Ma) periods are specified by tectonic, hydrogeological, climate changes and sea level variations (Butler et al., 1995; Rouchy et al., 2001; Flecker et al., 2015). During the Messinian salinity crisis (between 5.97 and 5.33 Ma) which can be described as deposition of thick evaporaites, these variations reached peak (Hsü et al., 1973; Krijgsman et al., 1999). During Neogene period, dolostone, gypsum, limestone, halite, marginal conglomerate and volcanic rocks deposited in the majority of East Mediterranean basins (Rozenbaum et al., 2019). Oligocene period is characterised by Red Sea opening (Zilberman and Calvo, 2013).

It is known that the age of the deep East Mediterranean basins are associated with the successive Tethys openings. The modern tectonic structure of the East Mediterranean Region can be linked to the evolution of the Neotethys Ocean (Ben-Avraham and Ginzburg, 1990; Robertson et al., 1991; Ben-Avraham et al., 2002). The Levant margin (Garfunkel and Derin, 1984; Ben-Avraham et al., 2002; Gardosh and Druckman, 2006; Colin et al; 2010; Gardosh et al., 2010; Hawie et al., 2013; Steinberg et al, 2018) and Egyptian margin (Camera et al., 2010; Yousef et al., 2010; Tari et al., 2012; Tassy et al., 2015) contain prominent stratigraphic constraints that shed light on the timing of formation of the deep basins in East Mediterranean (Tugend et al., 2019).

The Levant margin can be traced back to Late Triassic-Middle Jurassic period (Garfunkel, 2004; Gardosh and Druckman, 2006; Gardosh et al., 2010). NW-SE extension in the region is be supported by orientation of Eratosthenes Seamount, Levant and Egyptian margins (Garfunkel and Derin, 1984; Garfunkel, 2004; Gardosh and Druckman, 2006; Tari et al., 2012; Tassy et al., 2015).

There are many Permian marine basins along the Eastern Mediterranean (Stampfli et al., 2001; Guiraud et al., 2005; Frizon de Lamotte et al., 2013). These basins are located in northern Syria (Garfunkel, 1998), southern Tunisia, western central Sicily (Catalano et al., 1991) and eastern Crete (Robertson, 2006).

3. Methods

3.1. Curie point depth (CPD) estimation

Several methods can be used for CPD estimation: the centroid method (Okubo et al., 1985; Tanaka et al., 1999), spectral peak (Connard et al., 1983; Blakely, 1995) and forward modelling of the spectral peak (Ravat, 2004; Ross et al., 2006). These methods assume that the power spectrum of the infinite horizontal layer is a random function of x and y (Blakely, 1995; Cruz et al., 2020) and it is defined as:

$$A(k_x, k_y) = 2\pi\, C_m\, A_m\, |\theta_m|\, |\theta_f|\, e^{-k\, Z_t}\, (1 - e^{-k\,(Z_b - Z_t)}), \quad (1)$$

where k_x, and k_y are wavenumbers along x and y, C_m is the constant that related to proportionality, A_m is the amplitude spectrum, θ_m and θ_f define the direction of the magnetization and directional factor of the geomagnetic field, Z_b and Z_t are top and bottom depths of the magnetic source. If A_m is assumed as a constant and magnetization is counted as a random and uncorrelated function, Eq. (1) can be simplified by radial averaging:

$$A(k) = C\, e^{-k\, Z_t}(1 - e^{-k\,(Z_b - Z_t)}), \quad (2)$$

where C is a constant which is not dependent on the depth of magnetic source and k is $\sqrt{k_x^{\,2} + k_y^{\,2}}$.

Regarding the spectral peak method, Conrad (1983) suggested the following equation for the numerical solution:

$$\ln(Z_b - Z_t) = k_{peak}\,(Z_b - Z_t) \quad (3)$$

with k_{peak} is the wavenumber corresponding to the spectral peak. The major limitation of the method is spectral peak may not be detected.

The second method for the CPD estimation is the forward modelling of the spectral peak. Basically, the method reduces misfit between observed radial average power spectrum (RAPS) and synthetic RAPS with varying Z_b and Z_t. Similar to the spectral peak method, the forward modelling of the spectral peak cannot present reliable results if the peak is absent on the RAPS (Ravat, 2004; Ross et al., 2006; Ravat et al., 2007; Cruz et al., 2020).

The centroid method is the third method for the estimation of the bottom depth of the magnetic source. In this method, the top depth of the magnetic source is calculated from RAPS whereas depth to the centroid is estimated from the scaled RAPS. Top depth of the magnetic source (Z_t) can be calculated from (Spector and Grant, 1970; Bhattacharyya and Leu, 1975; Okubo et al., 1985; Tanaka et al., 1999; Li et al., 2010; Cruz et al., 2020):

$$\ln(A_k) \approx \ln(C) - kZ_t \quad (4)$$

If Eq. (2) is modified, depth to centroid of the magnetic source (Z_0) can be estimated as:

$$A(k) = D\, e^{-k\, Z_0}\, (e^{-k\,(Z_t - Z_0)} - e^{-k\,(Z_b - Z_0)}), \quad (5)$$

where D is a constant value. Modifications can be applied to Eq. (5) to simplify calculation of Z_0:

$$\ln(A_k / k) \approx \ln(D) - kZ_0 \quad (6)$$

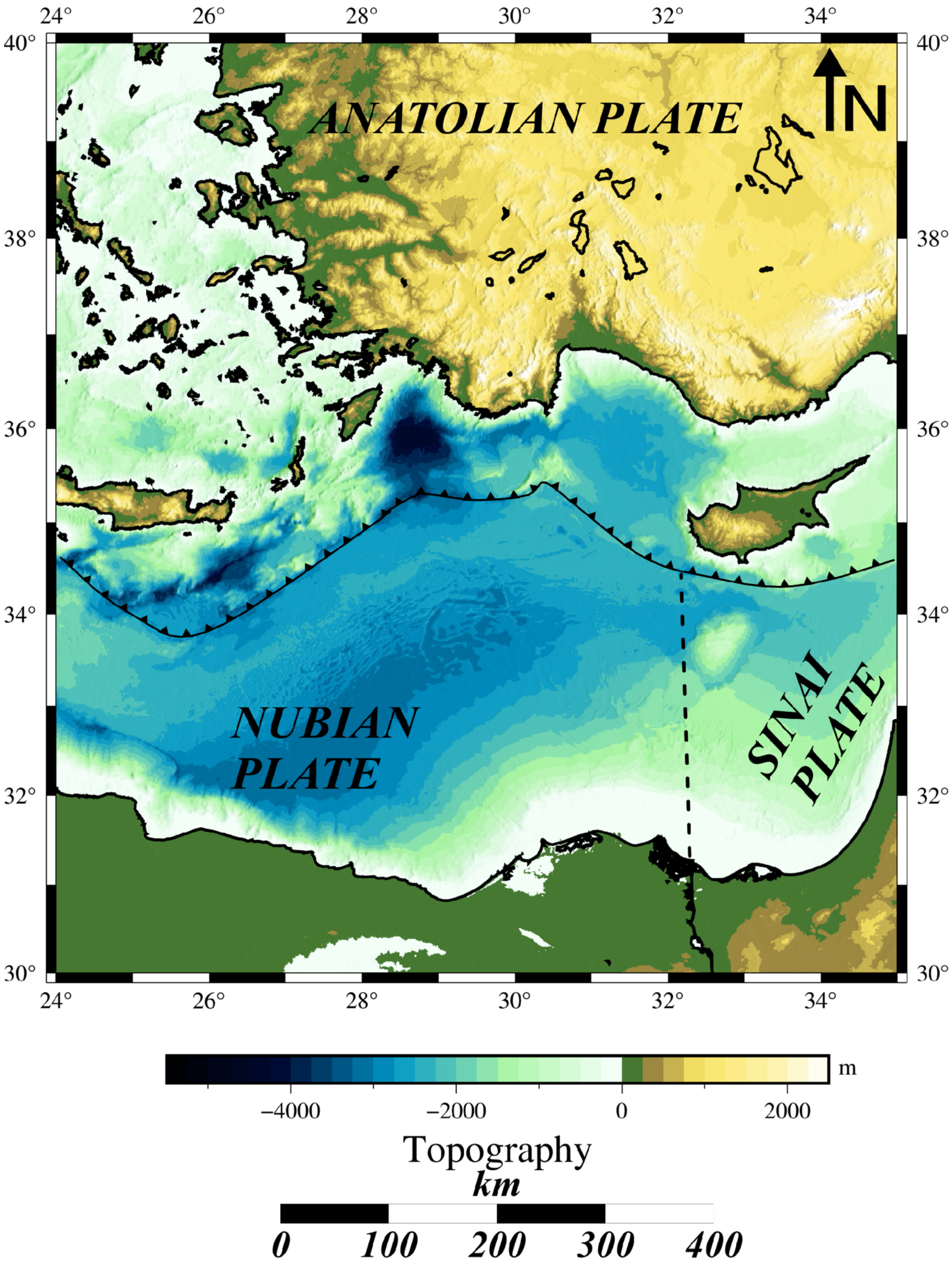

Figure 1. Simplified tectonic map of the study area.

It is obvious that Eqs. (4) and (6) can be solved by a linear fit. Z_t and Z_0 parameters are obtained from the slope of the linear estimation. Consequently, Z_b can be defined as:

$$Z_b = 2Z_0 - Z_t. \quad (7)$$

The uncertainty of estimated bottom depth of the magnetic source is calculated as (Martos et al., 2019; Cruz et al., 2020):

$$\Delta Z_b = \sqrt{2\,\Delta Z_0^{\,2} - \Delta Z_t^{\,2}}\,. \tag{8}$$

Alternatively, fractal magnetization parameter can be used for corrections on the power spectrum (Bouligand et al., 2009; Bansal et al., 2011; Li et al., 2013; Salem et al., 2014; Li et al., 2017; Martos et al., 2018; Kumar et al., 2020; Cruz et al., 2020). On the other hand, Ravat et al. (2007) suggested that the fractal model may yield overcorrection on the RAPS and unreliable results.

In this study, the centroid method without a fractal model is used for the bottom depth of the magnetic sources. The CPD estimations are calculated using Matlab based GUI MAGCPD proposed by Cruz et al. (2020).

Since CPD is linked to 580 °C for magnetite, the heat flow can be calculated by Fourier's law (Fourier, 1878):

$$q(z) = \lambda\ \frac{\partial T(z)}{\partial z}. \tag{9}$$

In order to solve the differential equation for conductive heat transfer (Martos et al., 2017), boundary limits should be taken into account. In this case, Z_b is set as CPD, T_c is Curie temperature (580 °C for magnetite), λ is thermal conductivity, which was used as 2.2 W/mK and T_0 is surface temperature, assumed as 20 °C. The modified equation is given as:

$$q_s = \frac{\lambda\,(T_c - T_0)}{Z_b}. \tag{10}$$

In Eq. (10), radiogenic heat production, mass advection, the temperature dependence of thermal conductivity and transient cooling are neglected (Ravat et al., 2016).

3.2. Moho depth estimations

In this study, Moho depth estimations are estimated by Airy-Heiskanen isostasy theory. Basically, the principle of isostasy theory is that topographic features on the surface are compensated by subsurface mass-density variations (Kirby, 2019). Airy (1855) and Heiskanen (1931) proposed major undulations on topography must be compensated by crust-mantle interface variations at a crustal thickness from sea level. The prominent assumption for this theory is crust and mantle has uniform densities. Airy-Heiskanen isostasy model can be computed for sea as:

$$t_{sea} = \frac{z_{bath}\,\Delta\rho_{cw}}{\Delta\rho_{mc}} + T. \tag{11}$$

where t_{sea} is estimated Moho depths for sea, T is the crustal thickness from sea level, assumed as 30 km, z_{bath} is water column depth, ρ_c is crustal density, assumed as 2.67 g/cm^3, ρ_w is density of water column, taken as 1.03 g/cm^3, ρ_m is mantle density, 3.3 g/cm^3. Hence, $\Delta\rho_{cw}$ and $\Delta\rho_{mc}$ are ρ_c - ρ_w and ρ_m - ρ_c respectively.

3.3. Earthquake distribution map

Distribution of the earthquakes in the study area shed light on tectonically active areas. Additionally, focal depth of earthquakes may distinguish brittle and ductile parts of the crust. Earthquake data were obtained from USGS Earthquake Catalog (USGS, 2021).

During the selection phase, 26°–33° East longitudes and 32°–39° North latitudes are bounded the study area. In order to map entire historical earthquake events within the study area, date of the earthquakes were not filtered. Likewise, focal depth was not constrained. However, minimum magnitude threshold is chosen as 2.5. Nonearthquake events were not selected.

4. Results

The magnetic data of the Eastern Mediterranean Region is obtained from the World Digital Magnetic Anomaly Map (WDMAM) (Lesur et al., 2016). The magnetic map is levelled to the mean sea level. Then the first order trend is removed and reduction to the pole is applied to the data for 4.60° ± 0.32° declination and 44.58° ± 0.21° inclination. RTP magnetic anomaly is presented in Figure 2.

As it can be seen from Figure 2, variations are smoother in land areas opposed to sea due to the fact that magnetic data is levelled to the mean sea level. The range of the RTP anomaly is between –100 nT and 130 nT.

The magnetic data is divided into 39 subareas by windows to calculate the CPD. Each subarea has 200 × 200 km size. The window shift is half of the size, 100 km, along only N-S direction. The computation zones for CPD is demonstrated in Figure 3.

CPD values (Z_b) and its interpolated uncertainty (Z_b $Error$) are estimated for 39 points. The mean Z_b $Error$ is ± 0.65 km. The calculated depths and uncertainties are mapped in Figure 4.

The estimated Curie point depths are varying from 4.5 km to 25 km. Mean CPD for the study area is 16.51 ± 7.60 km. Heat flow distribution is estimated through Fourier's law using CPD and Curie temperature (580 °C for magnetite). The heat flow map is shown in Figure 5. Heat flow results indicated that variations are between 55 mW/m^2 and 277 mW/m^2. For the study area, the expected heat flow value for the normal statistical distribution is 93.42 ± 43.67 mW/m^2.

Digital elevation data is obtained from SRTM30 (Farr et al., 2000; Rosen et al., 2000). The horizontal grid spacing is 30 arc s. For constraining the interpretation, Moho depth is calculated using Airy isostasy theory. Figure 6 indicates computed Moho depths. Since the computed Moho depths using Airy theory directly depend on the bathymetry data, the results should be compared to the previous studies for assessing the reliability of the results.

Vanacore et al. (2013) derived Moho map of Anatolian Plate using receiver function analysis and the results indicate that Moho depth is roughly 25 km in the southern part of Turkey. In this study, estimated Moho depth by Airy theory is 25–30 km for the same area. Additionally, Mechie et al. (2013) pointed out Moho depth ranges from approximately 15 km to 31 km in the eastern part of the study area. Similarly, estimated Moho depth in this study is roughly between 18 and 35 km. Furthermore, variation of the computed Moho depth is somewhat correlated with the mentioned previous studies. As a consequence, it might be said that calculated Moho depth, obtained by Airy theory, produces reliable results.

In order to evaluate the effect of sediment deposition on the observed RTP anomaly. The sediment thickness map is given in Figure 7. Sediment thickness map is obtained from CRUST 1.0 model (Laske et al., 2013). Distribution of the sediment accumulation zones are controlled by basement structure, age of the crust, tectonic history, nature of sediment and depocentre (Divins, 2003). The sediment thickness map

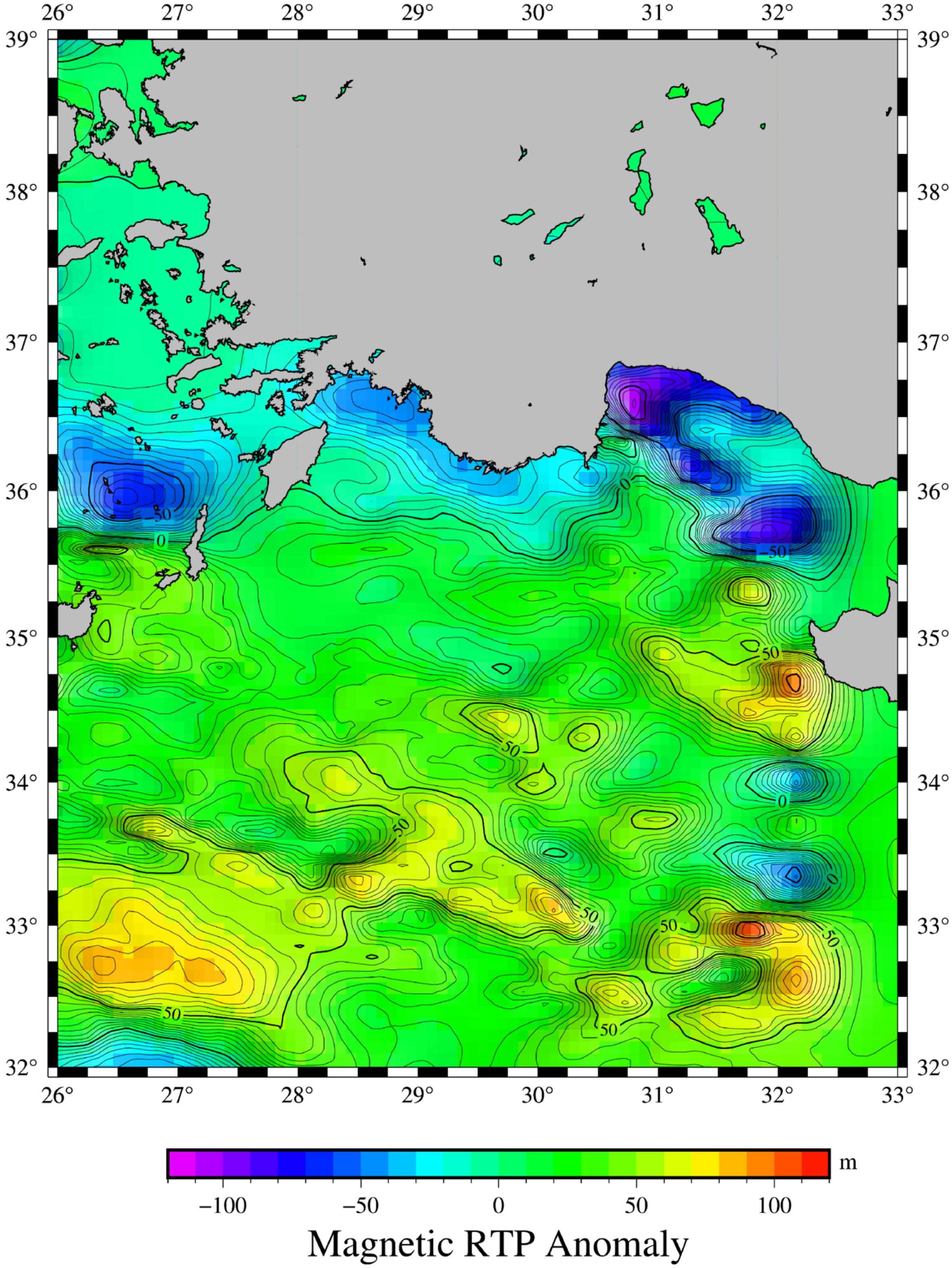

Figure 2. The RTP transformed magnetic anomaly of the study area.

was generated using drilling results and seismic profiles which provide depth to acoustic basement. The estimated sediment thickness from the seismic profiles reflects minimum thickness value since acoustic basement may not clearly present bottom depth of the sediments.

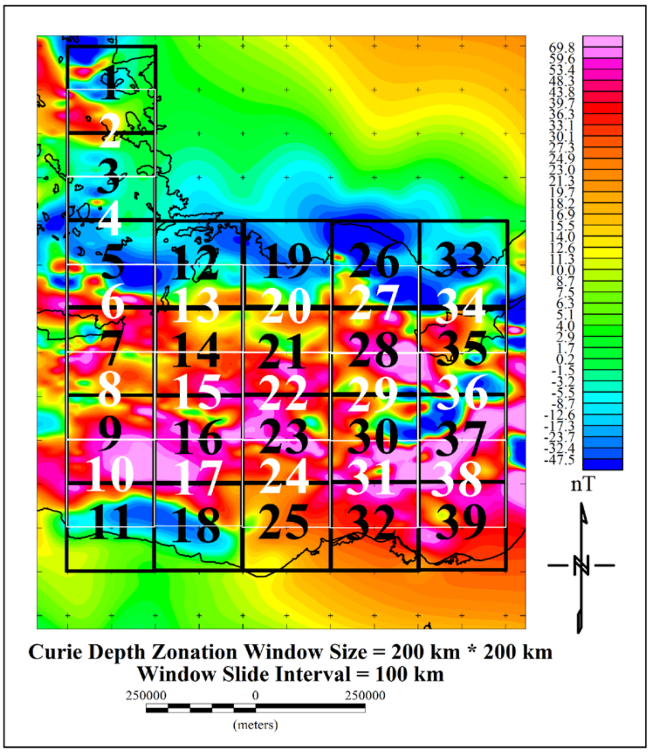

Figure 3. Curie point depth (CPD) zonation.

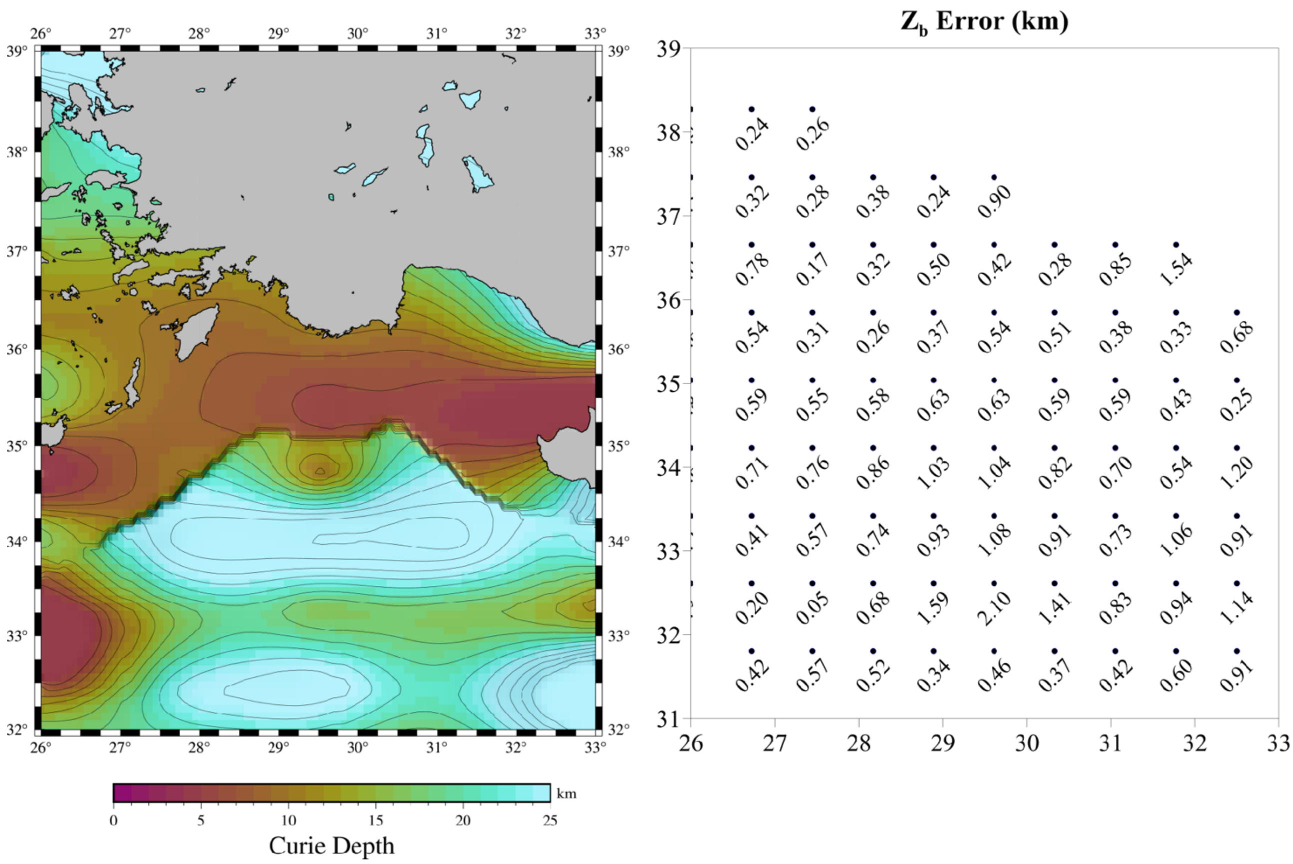

Figure 4. Map for the bottom depth (Zb) of the magnetic source and interpolated estimation error.

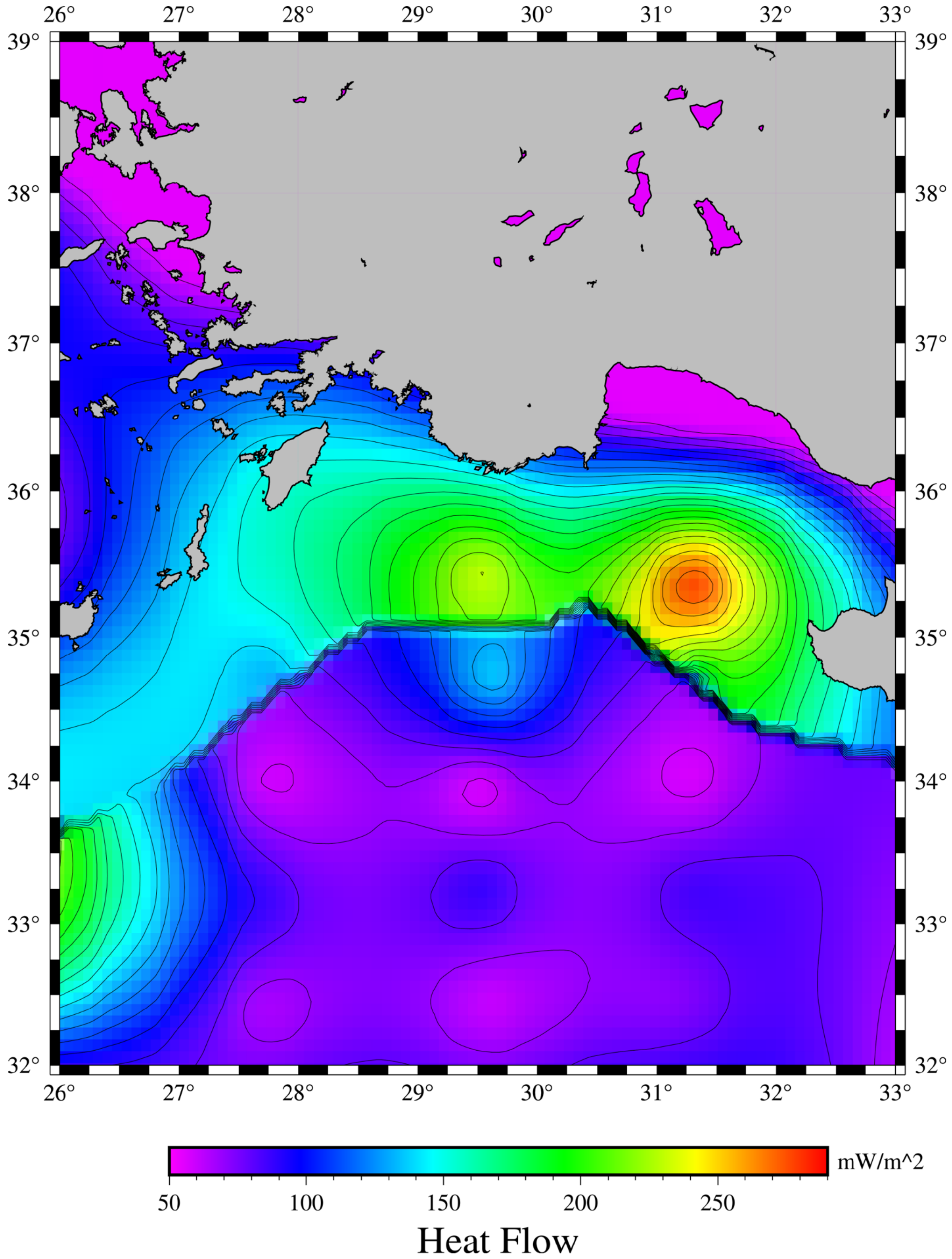

Figure 5. Heat flow map of the study area.

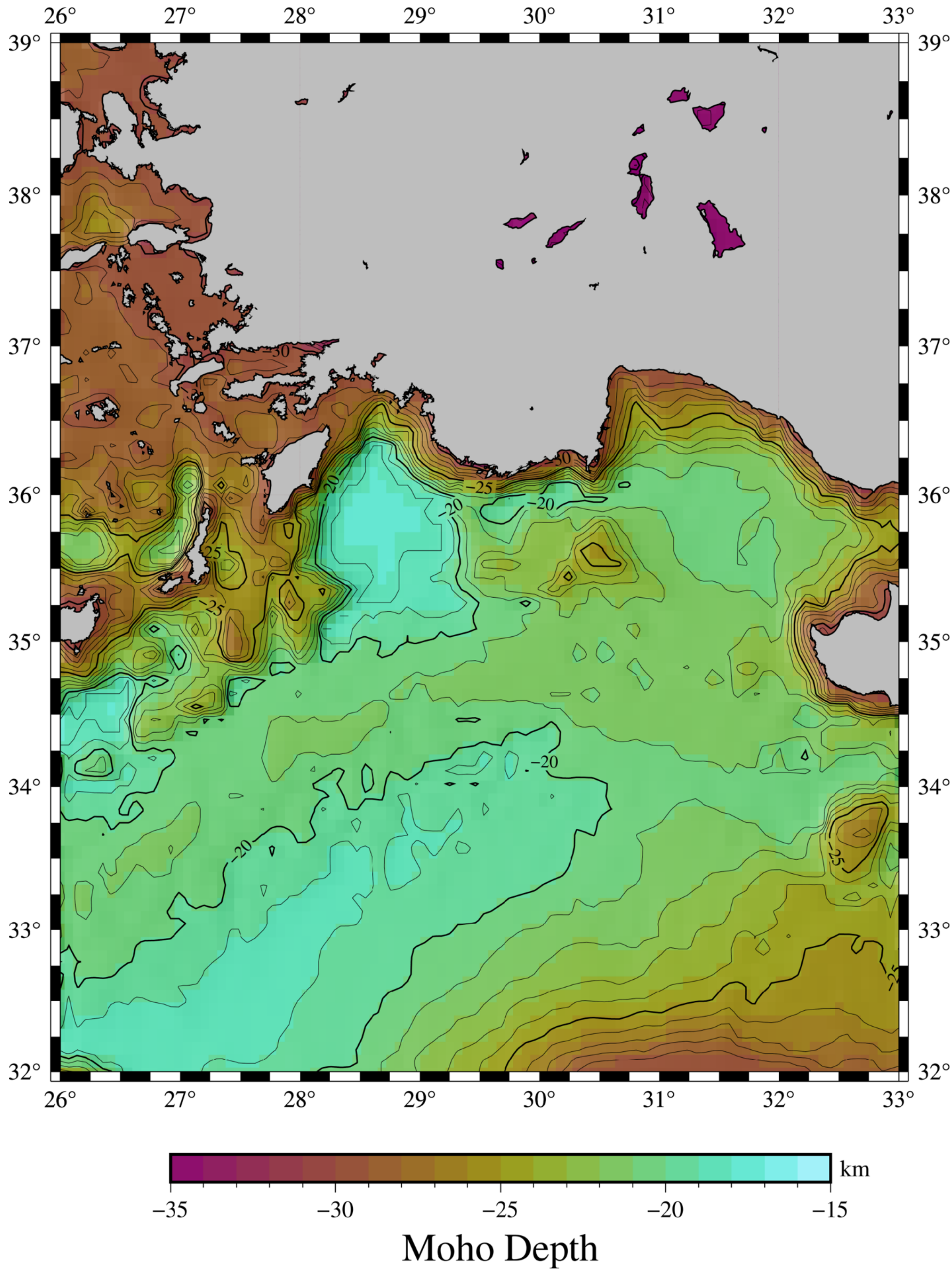

Figure 6. Estimated Moho depth for the study area. Contour interval is 5 km.

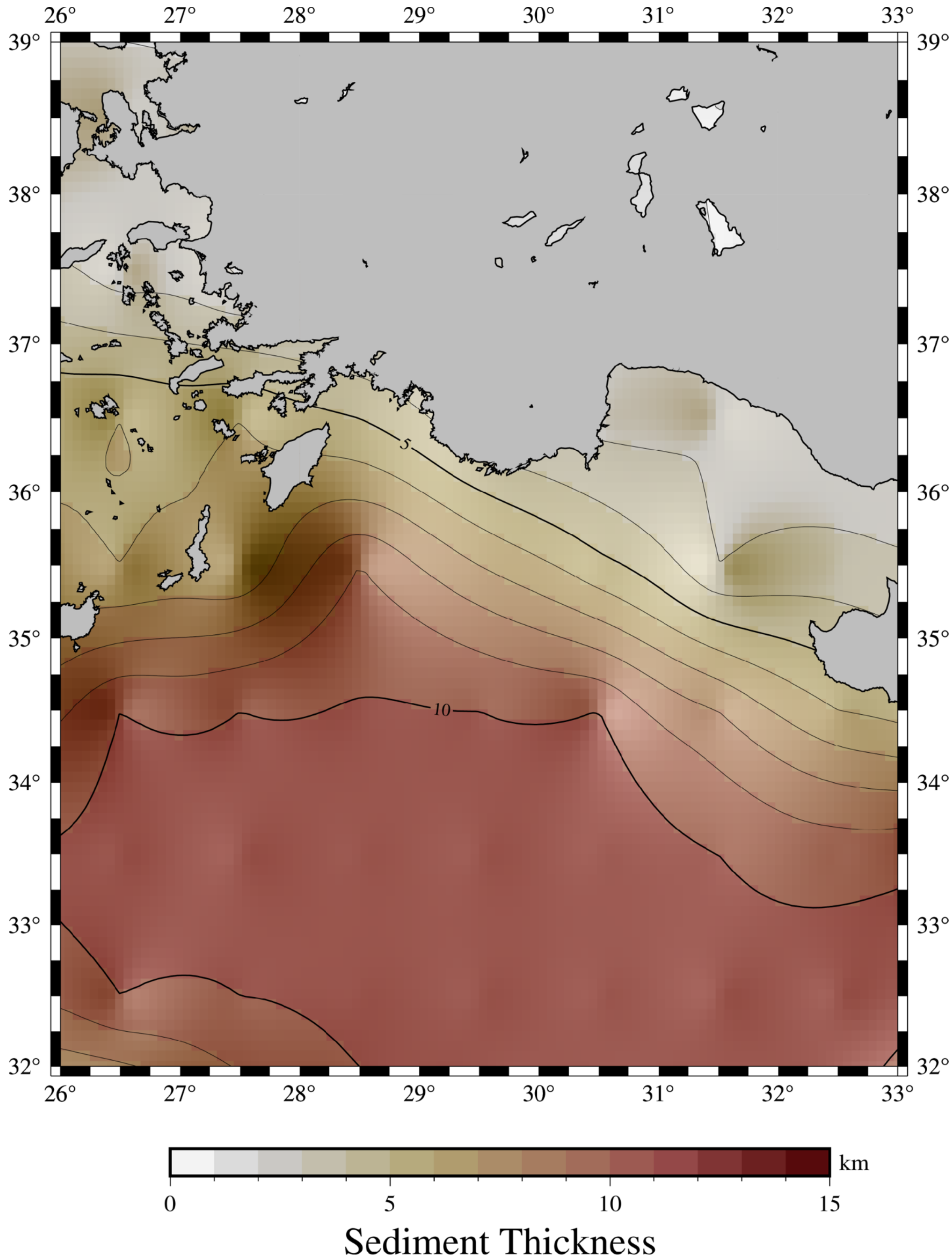

Figure 7. Sediment thickness map. Contour interval is 5 km.

5. Discussion and conclusion

Quantitative and qualitative interpretation are used to indicate possible hot, cold and active regions of the crust in the Eastern Mediterranean. Firstly, qualitative interpretation or nonautomated evaluation is preferred. Figure 8 shows the qualitative interpretation of the CPD and heat flow maps.

The computed CPD results are range from 4.5 to 25 km (Figure 4). In general, deeper CPD is estimated in the southern part of the study area, whereas shallower CPD is observed in the northern part. CPD values are deeper where crustal age of the ocean floor is relatively old. Even though it is not expected to observe 20–25 km CPD in the thin oceanic crust, it should be noted that Eastern Mediterranean is the oldest oceanic crust with approximately 240–260 Ma oceanic lithosphere age (Average age of the oceanic crust is 120–140 Ma) (Müller et al., 2008). Typically, sediment thickness, which increases the CPD and age of the lithosphere are positively correlated. Consequently, deep CPD values such as 20–25 km can be observed in the southern part of the study area, which has a distinctly old oceanic crust age.

It is possibly said that CPD and heat flow are negatively correlated (Figures 4 and 5) since radiogenic heat production, mass advection, the temperature dependence of thermal conductivity and transient cooling are ignored for calculation of the heat flow. For example, regions with a lower CPD is an indication for a higher heat flow. From a qualitative perspective, the southern part of the Eastern Mediterranean Ridge is characterised by deep CPD and low heat flow while high heat flow and shallow CPD are observed in the northern part of the East Mediterranean Ridge.

It might be said that oceanic crust is thin where heat flow values are higher than 100–110 mW/m^2. The thinnest crust in the study area is located just northern part of the East Mediterranean Ridge. From the tectonic perspective, East Mediterranean ridge forms a boundary between underlying African plate and overlying Eurasian plate. The African Plate underwent fractional melting during the subduction process. Then ascending mantle diapirs occur in the overlying crust. Consequently, the regions around the mantle diapirs reflect notably high heat flow and low CPD values.

The distance between the trench and fractional melting zone (or considerably high heat flow values) or the length of the forearc defines the dipping angle of the subduction mechanism. Sharp dipping can be interpreted where the length of the forearc is small while low dipping can be analysed for the high forearc length. In this study, the length of the forearc is fairly small since significantly high heat flow values are observed just northern part of the trench (Figure 5). Consequently, the results indicated that dipping angle of the African Plate might be quite sharp. It is prominent to note that data coverage should be uniform for determining the length of the forearc. Nevertheless, distribution of the WDMAM data points is not uniform. Thus, final decision about the dipping angle cannot be made from the WDMAM.

In Figure 8, the region between shallow and deep CPD presents different characteristics respect to the surrounding area. This midregion is specified by relatively high heat flow and shallow CPD. This distinct zone can be explained by the subduction mechanism between Eurasian plate and African plate. Since dipping angle of the African plate is assumed to be notably sharp, inflection points of the subducting plate tend to be deformed by stress. As a consequence, relatively hot crustal characteristics might be detected in this deformation zone (midregion). It should be emphasized that if additional geophysical constraints were available, more precise interpretation for the midregion would be achieved.

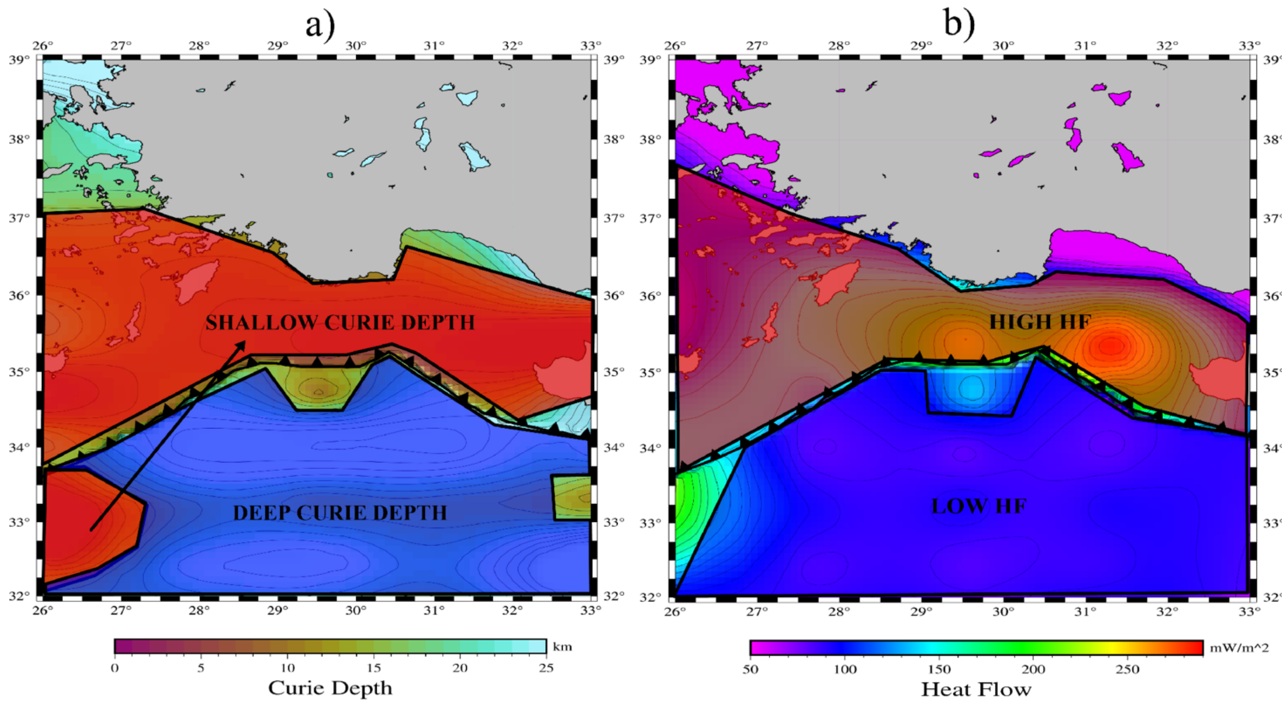

Figure 8. Nonautomated interpretation of the study area: a) CPD and b) heat flow.

Figure 9 illustrates Moho depth-CPD and its horizontal gradient. Difference between Moho depth and CPD and the first derivative of the difference could shed light on tectonically active and passive parts of the crust. If the difference between Moho depth and CPD produces local maxima and gradient fluctuates along N-S and E-W directions, the crust is probably considered as young and tectonically active. From a different perspective, local minima values of Moho-CPD and stable gradient across all directions are likely to indicate that old and passive region. The regions with abnormal characteristics (stable and unstable parts) are marked in Figure 9. It is underlined that marking stable-unstable parts of the crust is fairly biased and subjective without quantitative techniques.

The automated interpretation by quantitative techniques might produce more reliable results than qualitative (nonautomated) interpretation. In order to apply quantitative interpretation, boundary conditions should be set. Then binary format (0 and 1) is used for illustration of the results. To exemplify, 1 indicates regions where the boundary conditions are fulfilled and 0 denotes the areas which does not perfectly fit the boundary conditions. For cold parts of the crust, CPD >15 km (or < –15 km), Moho depth-CPD < 10 km (or > –10 km) and heat flow < 100 mW/m^2 used as boundary limits. The opposite conditions are set as a limit for evaluating hot crust. The gradient of the difference might be used for detecting tectonically active crust and |gradient| > 5° is used as a constraining parameter. Finally, earthquake focal depths are used for evaluating recent tectonic activity in the study area. The quantitative interpretation binary maps and earthquake distribution map are shown in Figure 10.

Regarding the automated estimation results, the southern part of East Mediterranean Ridge may be described as cold crust whereas the northern part is likely to be considered as a hot crust. Shallow earthquakes are expected in regions with hot crust due to deeper parts of the crust is ductile. On the contrary, the rigidity of the cold crust is relatively higher and it is characterised as a brittle medium.

If automated estimation results and earthquake distribution map is compared, better interpretation of the tectonic activity and rigidity of the crust will be obtained. It is important to note that earthquakes generally occur in brittle regime. Hence, focal depth of earthquakes provides crucial information about the brittle crust. Majority of the focal depths are 0–20 km which is somewhat compatible with the estimated CPD. Number of the earthquakes (Figure 10e) is dramatically greater in the northern part of the ridge than in the southern part. In other words, vast number of the earthquakes occurred in the area which was quantitatively interpreted as a hot crust (Figure 10b). Additionally, locations of the earthquakes generally correspond to the area where |gradient| is higher than 5° (Figure 10c).

Horizontal gradient of Moho depth-CPD indicates stable and unstable parts of the tectonic crust. The threshold for determining unstable parts is chosen as 5°. The unstable parts where the slope is higher than 5°, generally distributed in the northern part of the ridge. It might be said that tectonic crust around Crete presents higher slope values which indicate the tectonically active region. On the contrary, the southern part of the ridge is somewhat stable. The slope is generally lower than 5° and its variations are rare.

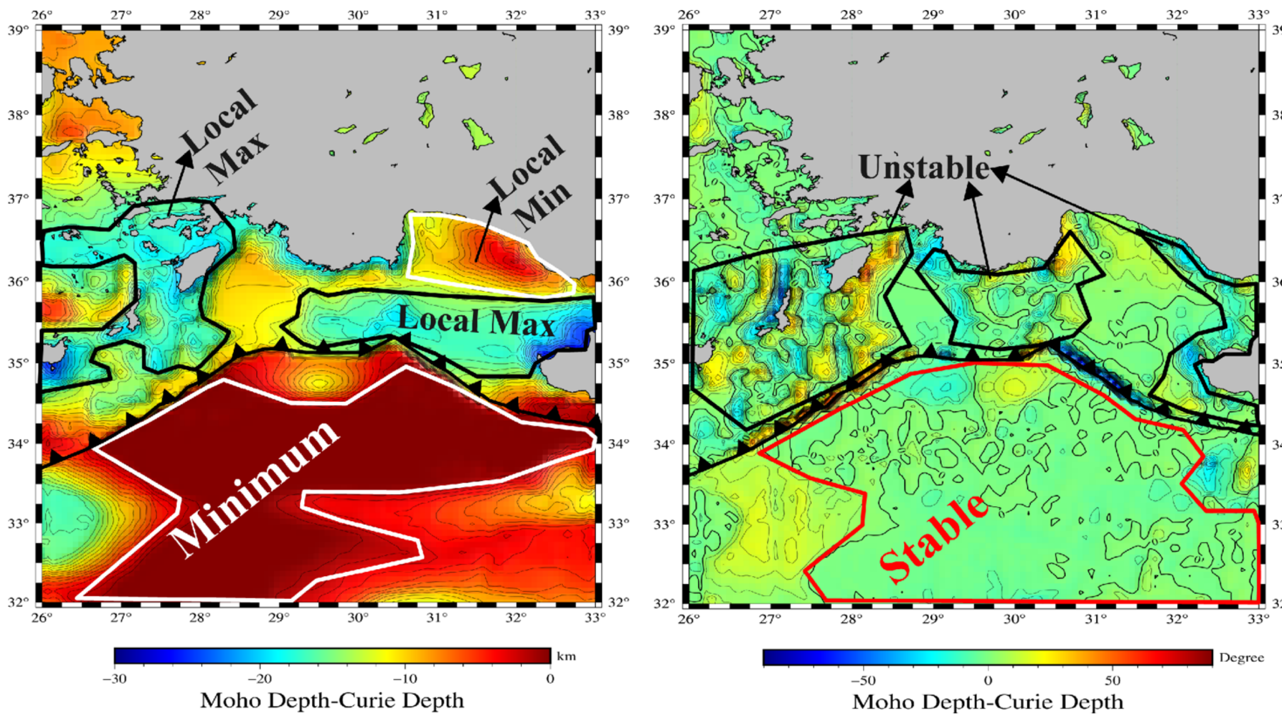

Figure 9. Maps for constraining quantitative interpretation (Results is multiplied with –1): a) difference between Moho depth and CPD, b) horizontal gradient of the difference.

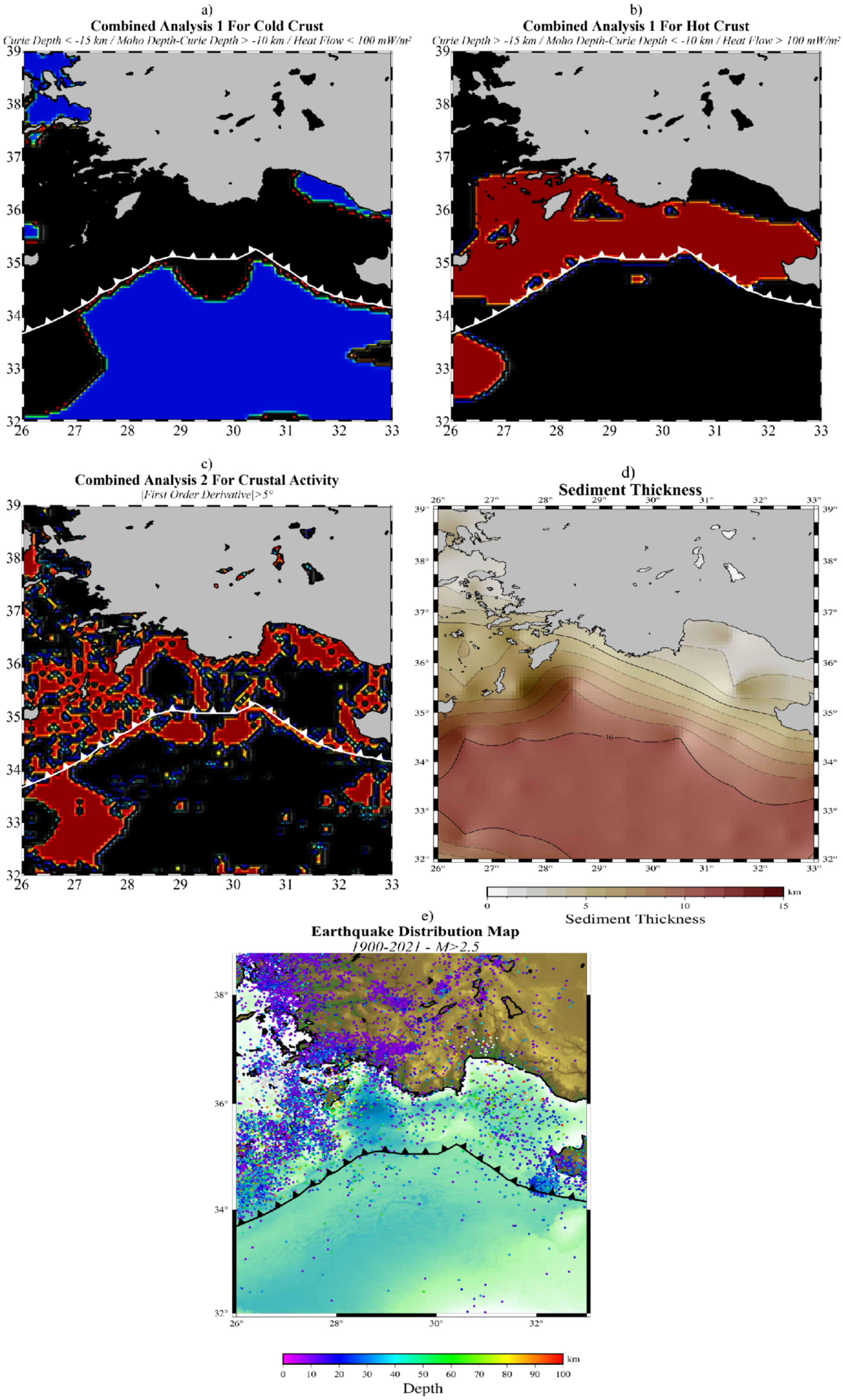

Figure 10. Automated interpretation for the study area. Quantitative interpretation binary map: a) cold (blue = 1, black = 0), b) hot (red = 1, black = 0), c) tectonically active (red = 1, black = 0) crust and d) sediment thickness, e) earthquake focal depth map.

Sediment thickness is decreasing from the south to the north. It is expected that sediment thickness is higher in the passive or cold tectonic crust. The cold crust indicated in quantitative interpretation corresponds to thick sediment accumulation. On the other hand, red colour in the automated interpretation corresponds to lower sediment thickness.

To sum up, the study area can be divided into two subareas in terms of CPD, thermal structure and sediment thickness. The Eastern Mediterranean Ridge formed E-W boundary between the subareas.

Cold crust characteristics are observed in the Aegean Sea but the results around the Western Anatolia is not reliable. Since window size is 200 × 200 km, only 4 windows are used for evaluation of the Northwest part of the study area. It is apparent that the increasing number of windows in the study area provides more reliable and credible results.

The northern part of the ridge becomes ductile at shallower depths. Consequently, shallow earthquakes are likely to occur. Moho-CPD gradient is notably higher in this part. Difference between CPD and Moho depth is bigger and undulations on the CPD are significant in the North which indicates unstable parts of the crust.

The southern part is relatively cold and thick. Sediment thickness is gradually increasing from the North to the South. Approximately constant Moho depth-Curie point depth values and gradient represent the crust that completes its tectonic activity.

Regarding the depth information, Helen, Pliny and Strabo trenches formed the deepest part of the Eastern Mediterranean with depths from 3500 to 4000 m (Gönenç and Akgün, 2012). Ates et al. (2012) provided about 25 km crustal thickness in the Southern Anatolia which is fairly similar to the Moho depth results and moderately correlated to the CPD result. Brocher (2005) computed crustal thickness of the Crete Island as 32–34 km. Furthermore, Snopek et al. (2007) indicated 40 km crust thickness around Peleponnese and 30 km for Crete Island. CPD is estimated about 3–5 km just southern part of the Crete Island while it is computed as 23–25 km just northern part of the island. The estimated CPD results are quite compatible with the literature for the northern part of the Crete Island. As a result, the southern and northern parts of the Crete Island present different crustal characteristics.

Eastern Mediterranean region is qualitatively and quantitatively interpreted in terms of CPD, thermal structure, tectonic activity and sediment thickness. It could be said that northern part of the Eastern Mediterranean ridge presents active tectonic characteristics with 4.5–8 km CPD, 130–277 mW/m^2 heat flow and 0–5 km sediment thickness. On the other hand, the older crust is observed in the southern region of the ridge by 15–25 km CPD, 50–100 mW/m^2 heat flow and 5–15 km sediment thickness. The given empirical data are the rough description of the results relative to the location of the ridge.

Future work is recommended for both the north and the south of the ridge. On the one hand, the southern part would be investigated by data with higher resolution in terms of past tectonic evaluation and sediment accumulation zones. On the other hand, the relationship between earthquakes and ductile parts of the tectonic plate movement in the Northern part could be studied.

Acknowledgments
I am extremely grateful to the anonymous reviewers for their constructive suggestions.

References

Airy GB (1855). III. On the computation of the effect of the attraction of mountain-masses, as disturbing the apparent astronomical latitude of stations in geodetic surveys. Philosophical Transactions of the Royal Society of London 145: 101-104. doi: 10.1098/rstl.1855.0003

Ateş A, Bilim F, Büyüksaraç A (2005). Curie point depth investigation of Central Anatolia, Turkey. Pure and Applied Geophysics 162 (2): 357-371. doi: 10.1007/s00024-004-2605-3

Ateş A, Bilim F, Büyüksaraç A, Aydemir A, Bektas O et al. (2012). Crustal structure of Turkey from aeromagnetic, gravity and deep seismic reflection data. Surveys in geophysics 33 (5): 869-885.

Aydemir A, Bilim F, Çifçi G, Okay S (2018). Modeling of the Foca-Uzunada magnetic anomaly and thermal structure in the gulf of Izmir, western Turkey. Journal of Asian Earth Sciences 156: 288-301.

Aydemir A, Bilim F, Kosaroglu S, Büyüksaraç A (2019). Thermal structure of the Cappadocia region, Turkey: a review with geophysical methods. Mediterranean Geoscience Reviews 1 (2): 243-254.

Aydın İ, Karat Hİ, Koçak A (2005). Curie-point depth map of Turkey. Geophysical Journal International 162 (2): 633-640. doi: 10.1111/j.1365-246X.2005.02617.x

Bansal AR, Gabriel G, Dimri VP, Krawczyk CM (2011). Estimation of depth to the bottom of magnetic sources by a modified centroid method for fractal distribution of sources: an application to aeromagnetic data in Germany. Geophysics 76 (3): L11-L22. doi: 10.1190/1.3560017

Ben-Avraham Z, Ginzburg A (1990). Displaced terranes and crustal evolution of the Levant and the eastern Mediterranean. Tectonics 9 (4): 613-622. doi: 10.1029/TC009i004p00613

Ben-Avraham Z (1978). The structure and tectonic setting of the Levant continental margin, Eastern Mediterranean. Tectonophysics 46 (3-4): 313-331. doi: 10.1016/0040-1951(78)90210-X

Ben-Avraham Z, Ginzburg A, Makris J, Eppelbaum, L (2002). Crustal structure of the Levant Basin, eastern Mediterranean. Tectonophysics 346 (1-2): 23-43. doi: 10.1016/S0040-1951(01)00226-8

Bhattacharyya BK, Leu LK (1975). Analysis of magnetic anomalies over Yellowstone National Park: mapping of Curie point isothermal surface for geothermal reconnaissance. Journal of Geophysical Research 80 (32): 4461-4465. doi: 10.1029/JB080i032p04461

Bilim F (2011). Investigation of the Galatian volcanic complex in the northern central Turkey using potential field data. Physics of the Earth and Planetary Interiors 185 (1-2): 36-43. doi: 10.1016/j.pepi.2011.01.001

Bilim F, Akay T, Aydemir A, Kosaroglu S (2016). Curie point depth, heat-flow and radiogenic heat production deduced from the spectral analysis of the aeromagnetic data for geothermal investigation on the Menderes Massif and the Aegean Region, western Turkey. Geothermics 60: 44-57. doi: 10.1016/j.geothermics.2015.12.002

Bilim F, Kosaroglu S, Aydemir A, Buyuksarac A (2017). Thermal investigation in the Cappadocia region, Central Anatolia-Turkey, analyzing curie point depth, geothermal gradient, and heat-flow maps from the aeromagnetic data. Pure and Applied Geophysics 174 (12): 4445-4458. doi: 10.1007/s00024-017-1666-z

Blakely RJ (1996). Potential Theory in Gravity and Magnetic Applications. 1st ed. New York, USA: Cambridge University Press.

Bouligand C, Glen JM, Blakely RJ (2009). Mapping Curie temperature depth in the western United States with a fractal model for crustal magnetization. Journal of Geophysical Research: Solid Earth 114 (B11): 1-25. doi: 10.1029/2009JB006494

Brocher TM (2005). Empirical relations between elastic wavespeeds and density in the Earth's crust. Bulletin of the Seismological Society of America 95 (6): 2081-2092. doi: 10.1785/0120050077

Buddington AF, Lindsley DH (1964). Iron-titanium oxide minerals and synthetic equivalents. Journal of Petrology 5 (2): 310-357. doi: 10.1093/petrology/5.2.310

Butler RW, Lickorish WH, Grasso M, Pedley HM, Ramberti L (1995). Tectonics and sequence stratigraphy in Messinian basins, Sicily: constraints on the initiation and termination of the Mediterranean salinity crisis. Geological Society of America Bulletin 107 (4): 425-439. doi: 10.1130/00167606

Caméra L, Ribodetti A, Mascle J (2010). Deep structures and seismic stratigraphy of the Egyptian continental margin from multichannel seismic data. Geological Society, London, Special Publications 341 (1): 85-97. doi: 10.1144/SP341.5

Carrillo-de la Cruz JL, Prol-Ledesma RM, Velázquez-Sánchez P, Gómez-Rodríguez D (2020). MAGCPD: a MATLAB-based GUI to Calculate the Curie Point-Depth Involving the Spectral Analysis of Aeromagnetic Data. Earth Science Informatics 13 (4): 1539-1550. doi: 10.1007/s12145-020-00525-x

Catalano R, Di Stefano P, Kozur H (1991). Permian Circumpacific Deep-Water Faunas from the Western Tethys (Sicily, Italy)—New Evidences for the Position of the Permian Tethys. Palaeogeography, Palaeoclimatology, Palaeoecology 87 (1-4): 75-108. doi: 10.1016/0031-0182(91)90131-A

Collin PY, Mancinelli A, Chiocchini M, Mroueh M, Hamdam W et al. (2010). Middle and Upper Jurassic Stratigraphy and Sedimentary Evolution of Lebanon (Levantine Margin): Palaeoenvironmental and Geodynamic Implications. Geological Society, London, Special Publications 341 (1): 227-244. doi: 10.1144/SP341.11

Connard G, Couch R, Gemperle M (1983). Analysis of Aeromagnetic Measurements from the Cascade Range in Central Oregon. Geophysics 48 (3): 376-390. doi: 10.1190/1.1441476

Dewey JF, Şengör AC (1979). Aegean and surrounding regions: complex multiplate and continuum tectonics in a convergent zone. Geological Society of America Bulletin 90 (1): 84-92. doi: 10.1130/0016-7606(1979)90<84:AASRCM>2.0.CO;2

Dewey JF (1988). Extensional Collapse of Orogens. Tectonics 7 (6): 1123-1139. doi: 10.1029/TC007i006p01123

Dewey JF, Hempton MR, Kidd WSF, Saroglu FAMC, Şengör AMC (1986). Shortening of Continental Lithosphere: The Neotectonics of Eastern Anatolia—A Young Collision Zone. Geological Society, London, Special Publications 19 (1): 1-36. doi: 10.1144/GSL.SP.1986.019.01.01

Divins D L (2003). Total Sediment Thickness of the World's Oceans and Marginal Seas: Boulder, Colorado, National Oceanic and Atmospheric Administration National Geophysical Data Center.

Dolmaz MN, Hisarlı ZM, Ustaömer T, Orbay N (2005a). Curie point depths based on spectrum analysis of aeromagnetic data, West Anatolian extensional province, Turkey. Pure and Applied Geophysics, 162 (3): 571-590. doi: 10.1007/s00024-004-2622-2

Dolmaz MN, Ustaömer T, Hisarlı ZM, Orbay N. (2005b). Curie point depth variations to infer thermal structure of the crust at the African-Eurasian convergence zone, SW Turkey. Earth, Planets and Space 57 (5): 373-383. doi: 10.1186/BF03351821

Elbarbary S, Zaher MA, Mesbah H, El-Shahat A, Embaby A (2018). Curie point depth, heat flow and geothermal gradient maps of Egypt deduced from aeromagnetic data. Renewable and Sustainable Energy Reviews 91: 620-629. doi: 10.1016/j.rser.2018.04.071

Erbek E, Dolmaz MN (2019). Investigation of the thermal structure and radiogenic heat production through aeromagnetic data for the southeastern Aegean Sea and western part of Turkey. Geothermics 81: 113-122. doi: 10.1016/j.geothermics.2019.04.011

Farr TG, Kobrick M (2000). Shuttle Radar Topography Mission Produces a Wealth of Data. Eos, Transactions American Geophysical Union 81 (48): 583-585. doi: 10.1029/EO081i048p00583

Flecker R, Krijgsman W, Capella W, De Castro Martíns C. Dmitrieva E et al. (2015). Evolution of the Late Miocene Mediterranean–Atlantic gateways and their impact on regional and global environmental change. Earth-Science Reviews 150: 365-392. doi: 10.1016/j.epsl.2017.01.029

Fourier J (1878). The analytical theory of heat. The University Press.

Frizon de Lamotte D, Tavakoli-Shirazi S, Leturmy P, Averbuch O, Mouchot N et al. (2013). Evidence for Late Devonian Vertical Movements and Extensional Deformation in Northern Africa and Arabia: Integration in the Geodynamics of the Devonian World. Tectonics 32(2):107-122. doi: 10.1002/tect.20007

Gardosh MA, Druckman Y (2006). Seismic Stratigraphy, Structure and Tectonic Evolution of the Levantine Basin, Offshore Israel. Geological Society, London, Special Publications 260 (1): 201-227. doi: 10.1144/GSL.SP.2006.260.01.09

Gardosh MA, Garfunkel Z, Druckman Y, Buchbinder B (2010). Tethyan Rifting in the Levant Region and Its Role in Early Mesozoic Crustal Evolution. Geological Society, London, Special Publications, 341 (1): 9-36. doi: 10.1144/SP341.2

Garfunkel Z, Derin B (1984). Permian-Early Mesozoic Tectonism and Continental Margin Formation in Israel and Its Implications for the History of the Eastern Mediterranean. Geological Society, London, Special Publications 17 (1): 187-201. doi: 10.1144/GSL.SP.1984.017.01.12

Garfunkel Z (1998). Constrains on the Origin and History of the Eastern Mediterranean Basin. Tectonophysics 298 (1-3): 5-35. doi: 10.1016/S0040-1951(98)00176-0

Garfunkel Z (2004). Origin of the Eastern Mediterranean Basin: A Reevaluation. Tectonophysics 391 (1-4): 11-34. doi: 10.1016/j.tecto.2004.07.006

Gasparini P, Mantovani MSM, Corrado G, Rapolla A (1979). Depth of Curie Temperature in Continental Shields: A Compositional Boundary. Nature 278 (5707): 845-846. doi: 10.1038/278845a0

Goldsworthy M, Jackson J, Haines J (2002). The continuity of active fault systems in Greece. Geophysical Journal International 148 (3): 596-618. doi: 10.1046/j.1365-246X.2002.01609.x

Gönenç T, Akgün M (2012). Structure of the Hellenic subduction zone from gravity gradient functions and seismology. Pure and Applied Geophysics 169 (7): 1231-1255. doi: 10.1007/s00024-011-0391-2

Guiraud R, Bosworth W, Thierry J, Delplanque A (2005). Phanerozoic geological evolution of Northern and Central Africa: an overview. Journal of African Earth Sciences 43 (1-3): 83-143. doi: 10.1016/j.jafrearsci.2005.07.017

Hawie N, Gorini C, Deschamps R, Nader FH, Montadert L et al. (2013). Tectono-stratigraphic evolution of the northern Levant Basin (offshore Lebanon). Marine and Petroleum Geology 48: 392-410. doi: 10.1016/j.marpetgeo.2013.08.004

Heiskanen W (1931). Isostatic tables for the reduction of gravimetric observations calculated on the basis of Airy's hypothesis. Bulletin géodésique 30 (1): 110-153. doi: 10.1007/BF03029991

Hisarlı ZM (1996). Determination of Curie Point Depths in Western Anatolia and Related with the Geothermal Areas. PhD Thesis, İstanbul University, İstanbul, Turkey.

Hunt CP, Moskowitz BM, Banerjee SK (1995). Magnetic properties of rocks and minerals. Rock Physics and Phase Relations: A Handbook of Physical Constants 3: 189-204.

Hsü KJ, Ryan WB, Cita MB (1973). Late Miocene desiccation of the Mediterranean. Nature 242 (5395): 240-244. doi: 10.1038/242240a0

Jackson J, McKenzie D (1988). The relationship between plate motions and seismic moment tensors, and the rates of active deformation in the Mediterranean and Middle East. Geophysical Journal International 93 (1): 45-73. doi: 10.1111/j.1365-246X.1988.tb01387.x

Kahveci M, Çırmık A, Doğru F, Pamukçu O, Gönenç T (2019). Subdividing the tectonic elements of Aegean and Eastern Mediterranean with gravity and GPS data. Acta Geophysica 67 (2): 491-500. doi: 10.1007/s11600-019-00270-w

Khain VE, Polyakova ID (2004). Oil and gas potential of deep-and ultradeep-water zones of continental margins. Lithology and Mineral Resources 39 (6): 530-540. doi: 10.1023/B:LIMI.0000046956.08736.e4

Kirby JF (2019). On the pitfalls of Airy isostasy and the isostatic gravity anomaly in general. Geophysical Journal International 216 (1): 103-122. doi: 10.1093/gji/ggy411

Krijgsman W, Hilgen FJ, Raffi I, Sierro FJ, Wilson DS (1999). Chronology, causes and progression of the Messinian salinity crisis. Nature 400 (6745): 652-655. doi: 10.1038/23231

Kumar R, Bansal AR, Ghods A (2020). Estimation of Depth to Bottom of Magnetic Sources Using Spectral Methods: Application on Iran's Aeromagnetic Data. Journal of Geophysical Research: Solid Earth 125 (3): e2019JB018119. doi: 10.1029/2019JB018119

Laske G, Masters G, Ma Z, Pasyanos M (2013). Update on CRUST1. 0—A 1-degree global model of Earth's crust. Geophysical Research Abstracts 15: 2658.

Le Pichon X, Angelier J (1979). The Hellenic arc and trench system: a key to the neotectonic evolution of the eastern Mediterranean area. Tectonophysics 60 (1-2): 1-42. doi: 10.1016/0040-1951(79)90131-8

Le Pichon X (1983). Land-locked oceanic basins and continental collision: The Eastern Mediterranean as a case example. In: Symposium on mountain building; Utrecht, the Netherlands: pp.201-211.

Lesur V, Hamoudi, Choi Y, Dyment J, Thébault E (2016). Building the second version of the world digital magnetic anomaly map (WDMAM). Earth, Planets and Space 68 (1): 27. doi: 10.1186/s40623-016-0404-6

Li CF, Lu Y, Wang J (2017). A global reference model of Curie-point depths based on EMAG2. Scientific Reports 7: 45129. doi: 10.1038/srep45129

Li CF, Shi X, Zhou Z, Li J, Geng J et al (2010). Depths to the magnetic layer bottom in the South China Sea area and their tectonic implications. Geophysical Journal International 182 (3): 1229-1247. doi: 10.1111/j.1365-246X.2010.04702.x

Li CF, Wang J, Lin J, Wang T (2013). Thermal evolution of the North Atlantic lithosphere: new constraints from magnetic anomaly inversion with a fractal magnetization model. Geochemistry, Geophysics, Geosystems 14 (12): 5078-5105. doi: 10.1002/2013GC004896

Lowrie W (2007). Fundamentals of Geophysics. 1st ed. New York, USA: Cambridge University Press.

Maden N (2012). One-dimensional thermal modeling of the eastern pontides orogenic belt (NE Turkey). Pure and Applied Geophysics 169 (1): 235-248. doi: 10.1007/s00024-011-0296-0

Martos YM, Catalán M, Galindo-Zaldivar J (2019). Curie Depth, Heat Flux, and Thermal Subsidence Reveal the Pacific Mantle Outflow Through the Scotia Sea. Journal of Geophysical Research: Solid Earth 124 (11): 10735-10751. doi: 10.1029/2019JB017677

Martos YM, Catalán M, Jordan TA, Golynsky A, Golynsky D et al. (2017). Heat flux distribution of Antarctica unveiled. Geophysical Research Letters 44 (22): 11-417. doi: 10.1002/2017GL075609

McClusky S, Balassanian S, Barka A, Demir C, Ergintav S et al. (2000). Global Positioning System constraints on plate kinematics and dynamics in the eastern Mediterranean and Caucasus. Journal of Geophysical Research: Solid Earth 105 (B3): 5695-5719. doi: 10.1029/1999JB900351

McKenzie D (1972). Active tectonics of the Mediterranean region. Geophysical Journal International 30 (2): 109-185. doi: 10.1111/j.1365-246X.1972.tb02351.x

McKenzie D (1978). Active tectonics of the Alpine—Himalayan belt: the Aegean Sea and surrounding regions. Geophysical Journal International 55 (1): 217-254. doi: 10.1111/j.1365-246X.1978.tb04759.x

Mechie J, Ben-Avraham Z, Weber MH, Götze HJ, Koulakov I et al. (2013). The distribution of Moho depths beneath the Arabian plate and margins. Tectonophysics 609: 234-249. doi: 10.1016/j.tecto.2012.11.015

Mercier JL, Sorel D, Vergely P, Simeakis K (1989). Extensional tectonic regimes in the Aegean basins during the Cenozoic. Basin Research 2 (1): 49-71. doi: 10.1111/j.1365-2117.1989.tb00026.x

Müller RD, Sdrolias M, Gaina C, Roest WR (2008). Age, spreading rates, and spreading asymmetry of the world's ocean crust. Geochemistry, Geophysics, Geosystems 9 (4). doi: 10.1029/2007GC001743

Nishitani T, Kono M (1983). Curie temperature and lattice constant of oxidized titanomagnetite. Geophysical Journal International 74 (2): 585-600. doi: 10.1111/j.1365-246X.1983.tb01890.x

Okubo Y, Graf RJ, Hansen RO, Ogawa K, Tsu H (1985). Curie point depths of the island of Kyushu and surrounding areas, Japan. Geophysics 50 (3): 481-494. doi: 10.1190/1.1441926

Pamukçu O, Akçığ Z, Hisarlı M, Tosun S (2014). Curie Point depths and heat flow of eastern Anatolia (Turkey). Energy Sources, Part A: Recovery, Utilization, and Environmental Effects 36 (24): 2699-2706. doi: 10.1080/15567036.2011.574194

Pamukçu. (2016). Geodynamic assessment of Eastern Mediterranean region: a joint gravity and seismic b value approach. Arabian Journal of Geosciences 9 (5): 360. doi: 10.1007/s12517-016-2347-4

Ravat D (2004). Constructing full spectrum potential-field anomalies for enhanced geodynamical analysis through integration of surveys from different platforms. AGUFM 2004: G44A-03.

Ravat D, Morgan P, Lowry AR (2016). Geotherms from the temperature-depth–constrained solutions of 1-D steady-state heat-flow equation. Geosphere 12 (4): 1187-1197. doi: 10.1130/GES01235.1

Ravat D, Pignatelli A, Nicolosi I, Chiappini M (2007). A study of spectral methods of estimating the depth to the bottom of magnetic sources from near-surface magnetic anomaly data. Geophysical Journal International 169 (2): 421-434. doi: 10.1111/j.1365-246X.2007.03305.x

Rızaoğlu T, Parlak O, Höck V, İşler, F (2006). Tectonic Development of the Eastern Mediterranean Region. Geological Society of London. doi: 10.1144/GSL.SP.2006.260.01.01

Robertson AHF (2006). Sedimentary evidence from the south Mediterranean region (Sicily, Crete, Peloponnese, Evia) used to test alternative models for the regional tectonic setting of Tethys during Late Palaeozoic-Early Mesozoic time. Geological Society, London, Special Publications 260 (1): 91-154. doi: 10.1144/GSL.SP.2006.260.01.06

Robertson AHF, Clift PD, Degnan PJ, Jones G (1991). Palaeogeographic and palaeotectonic evolution of the Eastern Mediterranean Neotethys. Palaeogeography, Palaeoclimatology, Palaeoecology 87 (1-4): 289-343. doi: 10.1016/0031-0182(91)90140-M

Rosen PA, Hensley S, Joughin IR, Li FK, Madsen SN et al. (2000).

Synthetic aperture radar interferometry. Proceedings of the IEEE 88 (3): 333-382. doi: 10.1109/5.838084.

Ross HE, Blakely RJ, Zoback MD (2006). Testing the use of aeromagnetic data for the determination of Curie depth in California. Geophysics 71 (5): L51-L59. doi: 10.1190/1.2335572

Rouchy JM, Orszag-Sperber F, Blanc-Valleron MM, Pierre C, Rivière M et al. (2001). Paleoenvironmental changes at the Messinian–Pliocene boundary in the eastern Mediterranean (southern Cyprus basins): significance of the Messinian Lago-Mare. Sedimentary Geology 145 (1-2): 93-117. doi: 10.1016/S0037-0738(01)00126-9

Rozenbaum AG, Sandler A, Stein M, Zilberman E (2019). The sedimentary and environmental history of Tortonian-Messinian lakes at the east Mediterranean margins (northern Israel). Sedimentary Geology 383: 268-292. doi: 10.1016/j.sedgeo.2018.12.005

Rozimant K, Büyüksaraç A, Bektaş Ö (2009). Interpretation of magnetic anomalies and estimation of depth of magnetic crust in Slovakia. Pure and Applied Geophysics 166 (3): 471-484. doi: 10.1007/s00024-009-0447-8

Salazar JM, Vargas CA, Leon H (2017). Curie point depth in the SW Caribbean using the radially averaged spectra of magnetic anomalies. Tectonophysics 694: 400-413. doi: 10.1016/j.tecto.2016.11.023

Salem A, Green C, Ravat D, Singh KH, East P et al. (2014). Depth to Curie temperature across the central Red Sea from magnetic data using the de-fractal method. Tectonophysics 624: 75-86. doi: 10.1016/j.tecto.2014.04.027

Shirani S, Kalateh AN, Noorollahi Y (2020). Curie point depth estimations for northwest Iran through spectral analysis of aeromagnetic data for geothermal resources exploration. Natural Resources Research 29 (4): 2307-2332. doi: 10.1007/s11053-019-09579-1

Şalk M, Pamukçu O, Kaftan I (2005). Determination of the Curie point depth and heat flow from MAGSAT data of Western Anatolia. Journal of the Balkan Geophysical Society 8 (4): 149-160.

Schenk CJ (2010). Petroleum Systems and Assessment of Undiscovered Oil and Gas Resources of the Levant Basin, Eastern Mediterranean. In: GEO 2010 European Association of Geoscientists & Engineers; Manama, Bahrain. pp. 248.

Schettino A, Turco E (2011). Tectonic history of the western Tethys since the Late Triassic. Bulletin 123 (1-2): 89-105. doi: 10.1130/B30064.1

Seyitoğlu G, Scott B (1991). Late Cenozoic crustal extension and basin formation in west Turkey. Geological Magazine 128 (2): 155-166. doi: 10.1017/S0016756800018343

Snopek K, Meier T, Endrun B, Bohnhoff M, Casten U (2007). Comparison of gravimetric and seismic constraints on the structure of the Aegean lithosphere in the forearc of the Hellenic subduction zone in the area of Crete. Journal of Geodynamics 44 (3-5): 173-185. doi: 10.1016/j.jog.2007.03.005

Spector A, Grant FS (1970). Statistical models for interpreting aeromagnetic data. Geophysics 35 (2): 293-302. doi: 10.1190/1.1440092

Stampfli GM, Borel GD (2002). A plate tectonic model for the Paleozoic and Mesozoic constrained by dynamic plate boundaries and restored synthetic oceanic isochrons. Earth and Planetary Science Letters 196 (1-2): 17-33. doi: 10.1016/S0012-821X(01)00588-X

Stampfli GM, Mosar J, Favre P, Pillevuit A, Vannay JC (2001). Permo-Mesozoic evolution of the western Tethys realm: The Neo-Tethys East Mediterranean basin connection. Mémoires du Muséum national d'histoire naturelle 186: 51-108.

Steinberg J, Roberts AM, Kusznir NJ, Schafer K, Karcz, Z (2018). Crustal structure and post-rift evolution of the Levant Basin. Marine and Petroleum Geology 96: 522-543. doi: 10.1016/j.marpetgeo.2018.05.006

Tanaka A, Okubo Y, Matsubayashi O (1999). Curie point depth based on spectrum analysis of the magnetic anomaly data in East and Southeast Asia. Tectonophysics 306 (3-4): 461-470. doi: 10.1016/S0040-1951(99)00072-4

Tari G, Kohazy R, Hannke K, Hussein H, Novotny B et al. (2012). Examples of deep-water play types in the Matruh and Herodotus basins of NW Egypt. The Leading Edge 31 (7): 816-823. doi: 10.1190/tle31070816.1

Tassy A, Crouzy E, Gorini C, Rubino JL, Bouroullec JL et al. (2015). Egyptian Tethyan margin in the Mesozoic: Evolution of a mixed carbonate-siliciclastic shelf edge (from Western Desert to Sinai). Marine and Petroleum Geology 68: 565-581. doi: 10.1016/j.marpetgeo.2015.10.011

Taymaz T, Jackson J, Westaway R (1990). Earthquake mechanisms in the Hellenic Trench near Crete. Geophysical Journal International 102 (3): 695-731. doi: 10.1111/j.1365-246X.1990.tb04590.x

Tugend J, Chamot-Rooke N, Arsenikos S, Blanpied C, Frizon de Lamotte, D (2019). Geology of the Ionian Basin and margins: A key to the East Mediterranean geodynamics. Tectonics 38 (8): 2668-2702. doi: 10.1029/2018TC005472

USGS (2021). Earthquake Catalogue [online]. Website https://earthquake.usgs.gov/earthquakes/search/ [accessed 31 May 2021].

Vanacore EA, Taymaz T, Saygin E (2013). Moho structure of the Anatolian Plate from receiver function analysis. Geophysical Journal International 193 (1): 329-337. doi: 10.1093/gji/ggs107

Yousef M. Moustafa AR, Shann M (2010). Structural setting and tectonic evolution of offshore north Sinai, Egypt. Geological Society, London, Special Publications 341 (1): 65-84. doi: 10.1144/SP341.4

Zilberman E, Calvo R (2013). Remnants of Miocene fluvial sediments in the Negev Desert, Israel, and the Jordanian Plateau: Evidence for an extensive subsiding basin in the northwestern margins of the Arabian plate. Journal of African Earth Sciences 82: 33-53. doi: 10.1016/j.jafrearsci.2013.02.006